Removal Pathways of Surface Nitrogen in a Steady-State NO + CO Reaction on Pd(110) and Rh(110): Angular and Velocity Distribution Studies†

Izabela I. Rzeźnicka,‡ Yunsheng Ma,§ Gengyu Cao,|| and Tatsuo Matsushima*,§

Graduate School of Environmental Earth Science, Hokkaido University, Sapporo 060-0810 Japan, Catalysis Research Center, Hokkaido University, Sapporo 001-0021 Japan, and Department of Chemical Physics, University of Science and Technology of China, Hefei 230026, China

Received: December 21, 2003; In Final Form: March 24, 2004

The angular and velocity distributions of desorbing products N_2 and CO_2 were studied in a steady-state NO + CO reaction on Pd(110) and Rh(110) by cross-correlation time-of-flight techniques. The CO_2 desorption sharply collimated along the surface normal on both surfaces. On the other hand, N_2 desorption on Pd(110) sharply collimated along about 40° off the surface normal in the plane along the [001] direction below around 650 K, yielding a translational temperature of about 3600 K. At higher temperatures, the normally directed desorption was relatively enhanced. On Rh(110), desorbing N_2 sharply collimated along the surface normal, yielding a translational temperature of about 2500 K. The inclined desorption was assigned to the decomposition of the intermediate, $N_2O(a) \rightarrow N_2(g) + O(a)$, and the normally directed component was proposed to be due to the associative desorption of adsorbed nitrogen atoms, $2N(a) \rightarrow N_2(g)$. The branching of these pathways was analyzed on Pd(110).

I. Introduction

Nitrous oxide, N_2O, is formed when the emissions from diesel or petrol engines (containing NO) are passed through catalytic converters with active metals such as rhodium and palladium.[1] N_2O is harmful and yields a remarkable greenhouse effect. Knowledge of the relation of N_2 and N_2O formation is requisite for improving such environmental catalysts. This paper reports the first separation of three removal pathways of surface nitrogen, i.e., the associative process of $2N(a) \rightarrow N_2(g)$, the intermediate decomposition of $N(a) + NO(a) \rightarrow N_2O(a) \rightarrow N_2(g) + O(a)$, and its desorption without decomposition.

In the pathway through the N_2O intermediate on Rh(110), desorbing N_2 is expected to collimate at 30−70° off the surface normal because such large collimation angles were observed in the N_2O decomposition.[2−6] However, neither inclined N_2 desorption nor N_2O production became noticeable up to about 1×10^{-4} Torr of NO. N_2 desorption always collimated along the surface normal, suggesting that the associative process is predominant.[7] On the other hand, on Pd(110), the inclined N_2 desorption and a significant amount of N_2O formation were observed in a wide pressure range, indicating that the pathway through the N_2O intermediate was operative except for high temperatures.

The overall reaction rate at the steady-state NO + CO reaction is mostly controlled by the dissociation of adsorbed NO.[8] No information of the removal of surface nitrogen can be obtained from kinetic measurements at the steady-state conditions. The angular and velocity distributions of desorbing products can provide information on the reaction sites and also product desorption processes.[9] These distributions do not directly involve the reaction rate and are always related to the product desorption step whenever any step becomes rate-determining.[5,10] Thus, the inclined N_2 desorption is useful for examining the reaction pathway of NO decomposition. In fact, from the inclined desorption and similar velocity distributions of desorbing N_2 in both NO and N_2O decompositions on Pd(110),[11−14] Ohno et al. concluded that the N_2 emission in NO decomposition proceeds through the intermediate $N_2O(a)$. However, the surveyed steady-state conditions were limited to around 2×10^{-7} Torr because of the use of an apparatus designed for angle-resolved temperature-programmed desorption (AR-TPD).[12,15] In the present work, angle-resolved steady-state desorption (AR-SSD) measurements were successfully performed for steady-state NO decomposition up to 1×10^{-4} Torr using a gas doser with a fine orifice and cross-correlation time-of-flight technique.

The angular and velocity distributions of desorbing products in the course of catalyzed reactions have been mostly analyzed with modulated molecular beams (MMB).[16] For NO decomposition on well-defined surfaces in an ultrahigh vacuum, the phase-sensitive detection technique with beam modulations was requisite so that the N_2 signal could be monitored in the high background due to NO decomposition on the reaction chamber wall.[17] Steady-state conditions, however, cannot be established for the reaction because of the periodical change of reactants on the surface. Similar ambiguities were also induced in AR-TPD work in the presence of reactant gases, in which simple TPD phenomena were not differentiated from kinetic behavior at the steady-state conditions.[18−20] Thus, neither angular nor velocity distributions have been reported under steady-state NO + CO reactions except for our earlier work.[12,15]

Isotope-tracer experiments have frequently been reported for mechanism studies of NO reduction. Belton et al. could not confirm in their isotope-TPD work that N_2O produced on Rh(111) yielded N_2.[21] Recently, Zaera and Gopinath reported that the replacement of surface $^{14}N(a)$ by $^{15}N(a)$ upon shifting

† Part of the special issue "Gerhard Ertl Festschrift".

* To whom correspondence should be addressed. Fax: +81-11-706-9120. E-mail: tatmatsu@cat.hokudai.ac.jp.

‡ Graduate School of Environmental Earth Science, Hokkaido University.

§ Catalysis Research Center, Hokkaido University.

|| University of Science and Technology of China.

10.1021/jp0379603 CCC: $27.50
Published on Web 06/08/2004

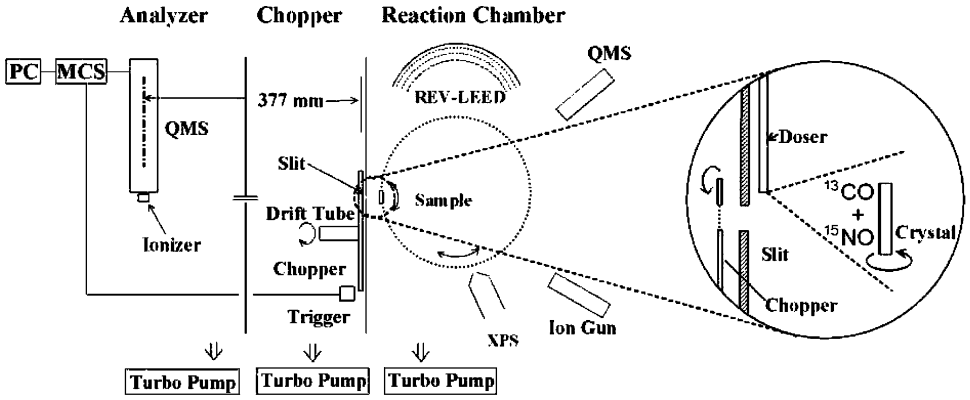

Figure 1. Apparatus for angle-resolved product desorption combined with cross-correlation time-of-flight techniques. The insert shows the structure around a sample crystal and a gas doser. REV-LEED (reverse-view low-energy electron diffraction optics); QMS (quadrupole mass spectrometer); XPS (X-ray photoelectron spectroscopy optics); MCS (multichannel scalar); trigger (photocell and light-emitting diode); PC (personal computer). The chopper house is pumped at about 7 $m^3\ s^{-1}$.

from ^{14}NO(g) to ^{15}NO(g) in a steady-state CO + NO reaction yielded $^{15}N_2$ and $^{14}N^{15}N$ in large amounts.[22] This result indicates that such isotope methods are not effective for differentiating the above N(a) removal processes.

II. Experiment

Experiments were performed in an ultrahigh-vacuum system composed of a reaction chamber, a chopper house, and an analyzer, which were separately pumped (Figure 1).[5,23] The reaction chamber is a conventional ultrahigh-vacuum chamber with a high pumping rate (about 1.5 $m^3\ s^{-1}$). It has reverse-view low-energy electron diffraction (LEED) and X-ray photoelectron spectroscopy (XPS) optics, a quadrupole mass spectrometer (QMS) for the angle-integrated (AI) form, an Ar^+ gun, a sample manipulator, and a gas-handling system. The chopper house has a narrow slit facing the reaction chamber and contains a cross-correlation random chopper blade.[24] The analyzer is equipped with another QMS operating in a pulse-counting mode for AR and time-of-flight (TOF) analyses. The arrival times at the ionizer of the QMS are registered in a multichannel scalar synchronized with the chopper rotation. The distance from the ionizer to the chopper blade is 377 mm. A time resolution of 20 μs is obtained with a chopper frequency of 98.023 Hz. A very large pumping rate is established in the chopper house by cooling a copper plate below 40 K, yielding about 7.0 $m^3\ s^{-1}$ of the pumping rate. Therefore, only molecules passing the first slit, the chopper slits, and the second drift tube without scattering can enter the ionizer of the analyzer. The analyzer is pumped by another turbo-molecular pump to keep the base pressure below 1×10^{-10} Torr. In this apparatus, AR-SSD measurements are possible up to 1×10^{-3} Torr.

A gas mixture of ^{15}NO and ^{12}CO or ^{14}NO and ^{13}CO was prepared in a glass bottle. The ^{15}NO/^{12}CO mixture was used in the experiment where the nitrogen signal was observed and the ^{14}NO/^{13}CO mixture was used when the CO_2 signal was monitored. One of the mixtures was introduced through a doser with a small orifice (diameter, 0.1 mm) about 2 cm from the sample crystal (the insert in Figure 1). Thus, the flux intensity of incident reactants decreases when the desorption angle shifts from the normal direction, where the desorption angle (polar angle, θ) is defined as the angle from the surface normal along the [001] direction. This effect was corrected as described in section III(A.2). The product signals due to $^{15}N_2$, $^{13}CO_2$, and $^{15}N_2O$ were monitored in both AI and AR forms. Hereafter, these species are simply described as N_2, CO_2, and N_2O in the text. The fragmentation of N_2O into N_2 in both mass spectrometers was separately estimated by introducing N_2O. It was only about 25% of the N_2O signal.

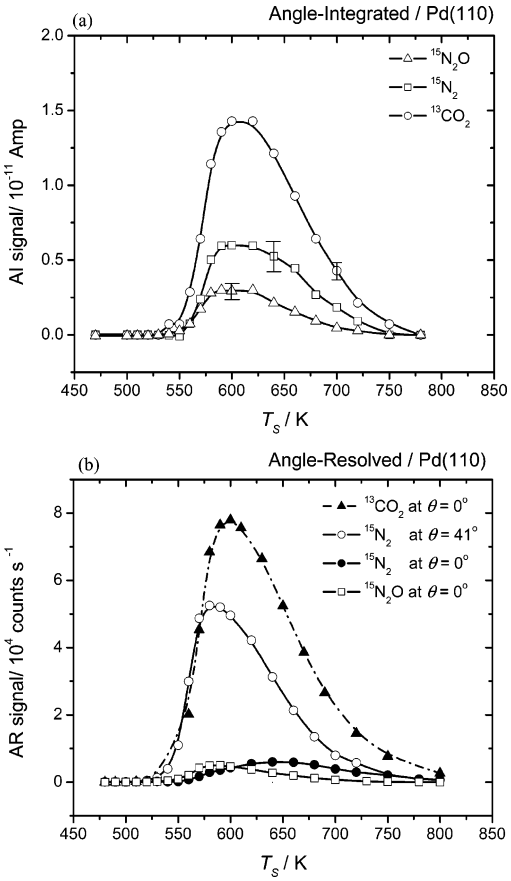

Figure 2. Steady-state reaction rate on Pd(110) versus surface temperature: (a) AI- and (b) AR-desorption signals of $^{13}CO_2$, $^{15}N_2O$ and $^{15}N_2$. The AR signals of $^{13}CO_2$, $^{15}N_2$, and $^{15}N_2O$ at $\theta = 0°$ and also of $^{15}N_2$ at $\theta = 41°$ off the surface normal toward the [001] direction are shown. The total pressure is 7.5×10^{-5} Torr (^{15}NO:^{12}CO = 1:1 or ^{14}NO:^{13}CO = 1:1). The lines in the figure are "guides to the eye".

III. Results

(A) Pd(110). *(A.1) General Features.* The steady-state formation rates of N_2, CO_2 and N_2O were monitored in both AI and AR forms as a function of the surface temperature (T_S), as shown in Figure 2. The effused flow of an equimolar mixture of NO and CO from the small orifice was kept constant, yielding the pressure in front of the crystal at around 7.5×10^{-5} Torr.

The AI signal (Figure 2a) was determined by the QMS in the reaction chamber as the difference in the signal between the desired surface temperature and room temperature. The mass sensitivity was corrected to each species. All the rates were negligible below 500 K, increased rapidly around 550 K to a maximum with increasing T_S, and decreased again at T_S values above 600 K. The AI N_2 signal was rather noisy because of the high background signal, which reached about 80% of the apparent total signal. Around the maximum rate, the ratio of CO_2:N_2:N_2O was 5:2.1:1. The N_2O formation was significant below 670 K.

The AR signal was obtained by the QMS in the analyzer as the difference between the signal at the desired angle and the signal when the crystal was away from the line-of-sight position. In Figure 2b, the AR signals at $\theta = 0°$ were shown for desorbing CO_2 and N_2O, and the AR signal at $\theta = 0$ and 41° is displayed for N_2 because these were their collimation angles (the maximum flux position), as described in section III(A.3). Similarly to the AI signals, the AR signals were negligible below 500 K; thereupon, those abruptly reached their maximum at about 600 K and slowly decreased toward zero at 800 K. No hysteresis was found in their rates with decreasing T_S values. The background N_2 signal level when the crystal was away was about 10% of the total signal at $\theta = 41°$ around 600 K.

Noticeable differences were found in the signal ratio between the AI and AR forms. These are explained by considering the differences in the sharpness of the angular distributions between each species below 600 K.[25] Above it, the ratio is also affected by changes in the branching of the surface nitrogen removal pathways with increasing T_S. These will be explained after the analysis of angular and velocity distributions.

Only the (1 × 1) pattern was observed in LEED measurements under a steady-state CO + NO reaction at the total pressure of 1×10^{-7} Torr of the equimolar mixture of NO and CO and in the range of $T_S = 400-800$ K. This is very different from the results in the CO + O_2 reaction on Pd(110), where LEED patterns changed from c(2×4)-O to (1×2)-CO and (1×1) with increasing CO pressure.[26]

(A.2) Angle-Resolved Measurements. A gas mixture of NO and CO was introduced through a gas doser with a small orifice at a constant flow rate (the inset of Figure 1). The use of this orifice was effective in reducing N_2 formation on the reaction chamber wall. Its formation with a NO dosage in the back-fill type is usually high and obscures the observation of N_2 formation on a small sample surface. The AR signal was slightly improved under this construction. For the steady-state CO + O_2 reaction, however, this construction was not necessarily requisite.[23] Under this construction, the flux of incident reactants toward the unit surface area decreases proportionally to the cosine of the desorption angle when the angle is shifted from the normal direction even if the incident reactant density in the effused beam is homogeneous around the crystal sample.

We examined this point in the following way. Here, two factors must be examined toward the surface composition: one is the decrement of the incident flux, and the other is the incident angle dependence of the adsorption rate. The latter factor is negligible because no incident angle dependence is expected for both CO and NO, which have the sticking probability close to unity on Pd(110) and Rh(110).[27]

To examine the former factor, the angular distribution of N_2O was measured at a fixed flow of the mixed gas. The results are shown in Figure 3a. The apparent AR signal of N_2O, without correction due to the increase of the surface area falling into the acceptance angle of the analyzer, closely followed a form

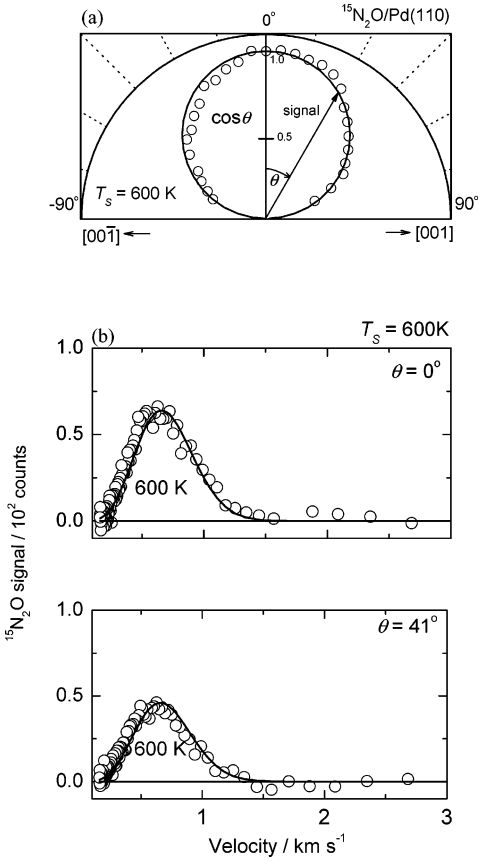

Figure 3. (a) Apparent angular distributions of desorbing $^{15}N_2O$ and (b) its velocity distributions at different desorption angles in the steady-state ^{15}NO + ^{12}CO reaction on Pd(110). The total pressure is 7.5×10^{-5} Torr (^{15}NO:^{12}CO = 1:1). The signal was not corrected by considering the changes in the reactant density and the surface area falling into the acceptance angle of the analyzer (see the text).

of cos(θ). The apparent signal should be invariant when the distribution is in a cosine form, and the incident flux is constant because the surface area falling into the acceptance angle increases as the reciprocal of the cosine of the desorption angle. The velocity of this product showed the Maxwellian distribution at the surface temperature at any desorption angle (Figure 3b). The cosine distribution is characteristic of the desorption after thermalization of molecules to the surface temperature.[24] Resultant desorbing molecules show a Maxwellian velocity distribution at the surface temperature all over the desorption angle. Here, we concluded that the density of the incident reactants around the sample crystal in the effused beam was homogeneous and then its incident flux to the unit area decreased in a form of cos(θ) when the angle was shifted from the normal direction. This effect must be considered in the angle-dependence analysis. However, the shift due to this correction was not significant.

(A.3) Angular Distributions. The AR signals of desorbing CO_2 and N_2 were sensitive to the desorption angle θ. CO_2 desorption sharply collimated along the surface normal, whereas the latter peaked around 40° off the surface normal toward the [001] direction. Assuming the power series of the cosine of the desorption angle to each desorption component,[5] the CO_2 signal was approximated in a form of $\cos^{13}(\theta)$ at $T_S = 550$ K and 7.5×10^{-5} Torr with the (1:1) mixture (Figure 4a). The sharp distribution became slightly broader as $\cos^8(\theta)$ at 650 K. On the other hand, the angular distribution of desorbing N_2 was in a two-directional form approximated as $\cos^{28}(\theta + 41) + \cos^{28}(\theta - 41)$ (Figure 5a). The signal at the normal direction was negligibly small at 550 K. A sharp two-directional form

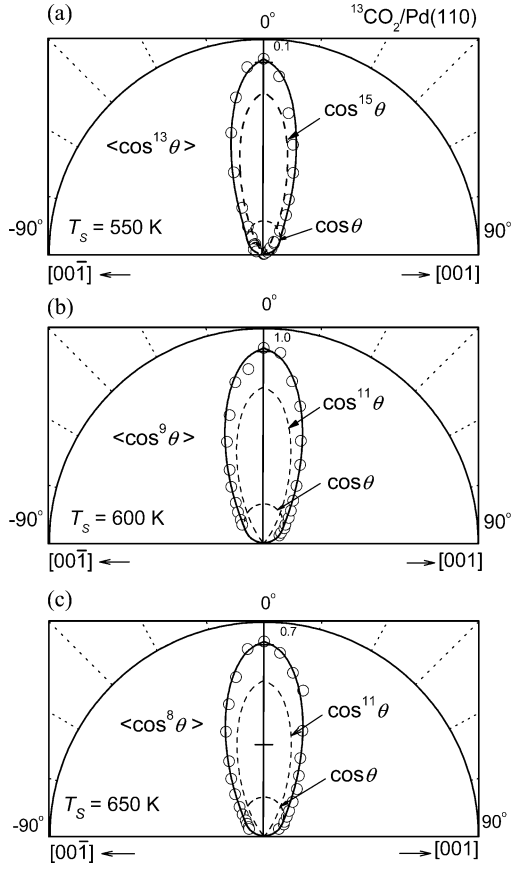

Figure 4. Angular distributions (shown in polar coordinates) of desorbing $^{13}CO_2$ in the plane along the [001] direction at different T_S values. The signal on the ordinate was normalized to that in the normal direction at 600 K. The reaction of $^{14}NO + {}^{13}CO$ on Pd(110) was at the steady state with the total pressure of 7.5×10^{-5} Torr (^{14}NO:^{13}CO = 1:1). The apparent distribution sharpness is indicated in $\langle\ \rangle$. Typical deconvolutions are drawn by broken curves. The solid lines show the summation of components.

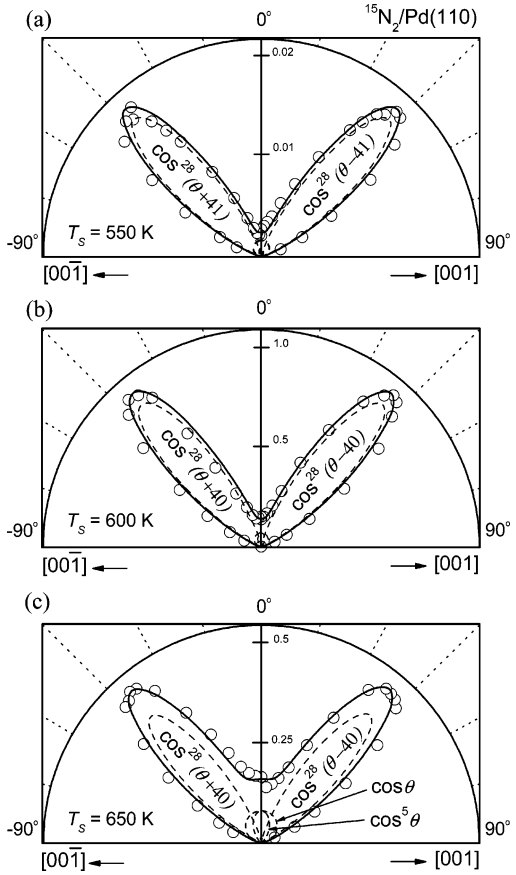

Figure 5. Angular distributions of desorbing $^{15}N_2$ in the plane along the [001] direction at different T_S values. The signal on the ordinate was normalized to the maximum at the collimation angle of $\theta = 40°$ and at 600 K. The reaction of $^{15}NO + {}^{12}CO$ on Pd(110) was at the steady state with the total pressure of 7.5×10^{-5} Torr (^{15}NO:^{12}CO = 1:1). Typical deconvolutions are drawn by broken curves. The solid lines show the summation of components.

collimated around ±40° is consistent with the previous results at 2×10^{-7} Torr.[12,15] The distributions at $T_S = 600$ and 650 K are shown in Figure 5b,c. With increasing T_S, the inclined desorption signal decreased at T_S values higher than 600 K, but it was still significant at 700 K. The collimation angle of the inclined desorption slightly decreased at higher T_S. The signal intensity at the normal direction increased with increasing T_S, indicating the presence of the normally directed component. The total signal at 650 K was approximated by $0.85\{\cos^{28}(\theta + 40) + \cos^{28}(\theta - 40)\} + 0.16\cos^5(\theta) + 0.16\cos(\theta)$ as referred to the velocity analysis in the next section.

(A.4) Velocity Distributions. Both desorbing CO_2 and N_2 showed hyperthermal energy. The translational temperature of N_2 was very high, more than twice that of CO_2. Typical velocity curves of N_2 are shown in Figure 6. The apparent translational temperature calculated from the average kinetic energy ($\langle E\rangle$) as $T_{\langle E\rangle} = \langle E\rangle/2k$, is shown in $\langle\ \rangle$ in the figure, where k is the Boltzmann constant. The value was maximized around the collimation angle to the value of 3570 K at $T_S = 550$ K (Figure 6a) and a similar value at $T_S = 650$ K (Figure 6b). It decreased quickly with an increasing shift from the collimation angle. The value at the normal direction decreased to 1100 K at $T_S = 550$ K. It was highly underestimated because of the relatively high background signal. The angle dependence is consistent with the inclined desorption.

The velocity distributions of CO_2 at $T_S = 550$ and 650 K are shown at different desorption angles in Figure 7. The average translational temperature was around 1600 K, about 3 times higher than the surface temperature at the normal direction and decreased quickly with an increasing desorption angle, being consistent with the normally directed distribution.[28,29] The values slightly increased with T_S. On the other hand, desorbing N_2O showed a Maxwellian distribution at the surface temperature.

(B) Rh(110). *(B.1) Temperature Dependence.* The maximum N_2 or CO_2 formation rate on Rh(110) was about 1 order less than that on Pd(110). However, the Rh (110) surface showed noticeable activity already around 450 K, where no activity was found on Pd(110). Thus, it became difficult to determine the AI N_2 signal on Rh(110) because of the relatively enhanced background. On this surface, a pronounced hysteresis was observed in the reaction rate with surface temperature changes. Figure 8 shows the AR signals of products N_2 and CO_2 at their collimation angle $\theta = 0°$ under steady-state conditions at the total pressure of 7.5×10^{-5} Torr. No detectable N_2O formation was found under these conditions. For both CO_2 and N_2 products, the formation rate was negligible below 400 K and then suddenly increased around 450 K, reaching the first maximum at 580−590 K. After this maximum, the rate once decreased and started to increase again around 700 K, reaching the second maximum at 740 K. Above it, the rate slowly decreased. When the surface temperature decreased, the rate was reproduced at the second maximum around 740 K. It started to decrease around 600 K and did not reach the first maximum around 580 K. The reaction was highly retarded below 600 K when the surface was cooled. A similar hysteresis was also

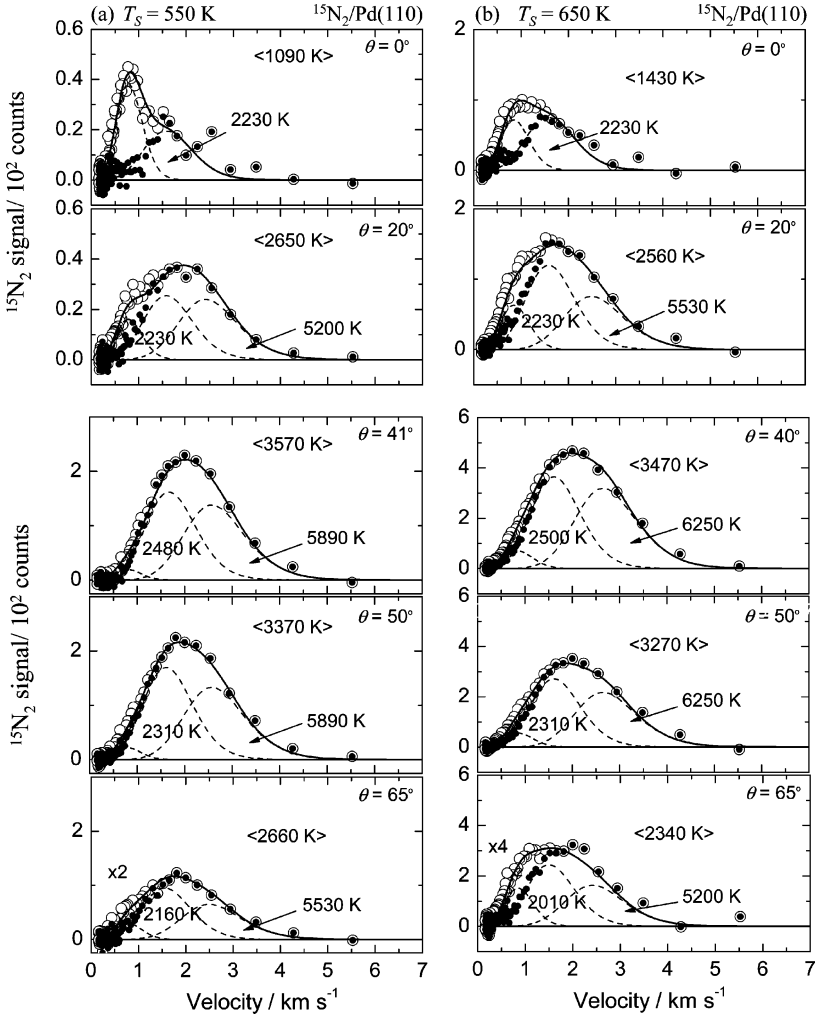

Figure 6. Velocity distributions of desorbing $^{15}N_2$ at various desorption angles in a steady-state $^{15}NO + {}^{12}CO$ reaction on Pd(110) at the total pressure of 7.5×10^{-5} Torr (^{15}NO:^{12}CO = 1:1) at (a) T_S = 550 K and (b) T_S = 650 K. The angle θ was scanned in the plane along the [001] direction. The average kinetic energy is given in $\langle\ \rangle$ in temperature units. Typical deconvolutions into two fast components and a slow component are given by broken curves. The translational temperature for each component is also given. Open circles represent observed signals, and closed ones indicate the signals after subtraction of the thermalized component.

found in the CO_2 formation rate (Figure 8b). A sharp increase in the CO_2 signal was observed around 470 K at the jump position of the N_2 signal before the first N_2 maximum at 590 K. This CO_2 spike was reproducible, and the intensity was kept constant; however, it was difficult to see a similar spike in the N_2 signal because of the high background. The spike in the N_2 signal was more pronounced when more NO was in the mixture gas. The CO_2 formation was also reduced below 600 K when the surface was cooled.

In LEED measurements at the total pressure of 1×10^{-7} Torr with the (1:1) mixture gas, a (2×1) pattern appeared at 360 K, where no reaction proceeded (Figure 9). It was due to NO adsorption, mostly to reconstruction by N adsorption.[30] It was transformed into a (3×1) pattern due to reconstruction by N(a) at 380−400 K. At 400 K, a mixed pattern of (2×1) and (1×3) appeared. Above 600 K, it transformed into a (1×2) pattern. In the direction of surface cooling, the (1×2) pattern was stable up to 620 K, and then a mixed pattern of (1×3) and c(4×2) was observed. These are similar to those observed by oxygen adsorption.[31] The retardation seems to be due to surface oxide formation.

(B.2) Angular and Velocity Distributions. Both N_2 and CO_2 products desorbed sharply along the surface normal over the conditions studied. The N_2 desorption became sharper with increasing T_S at the total pressure of 7.5×10^{-5} Torr with the (1:1) mixture, from $\cos^2(\theta)$ at 470 K to $\cos^7(\theta)$ at 750 K (Figure 10a). On the other hand, the sharpness of the CO_2 distribution was insensitive to the T_S value approximated as $\cos^3(\theta)$.

The velocity distributions of desorbing N_2 showed the average translational temperature around 2600−2700 K, which was surprisingly insensitive to the desorption angle, as shown in Figure 11a. It increased with increasing surface temperature with a slope of about 2 (Figure 12a). The average CO_2 translational temperature reached around 1310 K at the surface normal direction at T_S = 470 and 1920 K at 750 K (Figure 12b). The value increased with increasing surface temperature with a slope similar to that of N_2. It decreased quickly with increasing desorption angle, consistent with the normally directed desorption (Figure 13).

IV. Discussion

(A) Desorption Components. *(A.1) Pd(110).* The velocity distributions of CO_2 and N_2 products showed different features. The distribution of desorbing N_2 is too broad as a single desorption component. To examine this point, the thermalized component to the surface temperature was first subtracted from the observed distribution. The presence of this thermalized one is clear from the data at $\theta = 0°$ as shown in Figure 6a,b. The resultant distributions yielded the translational temperature of

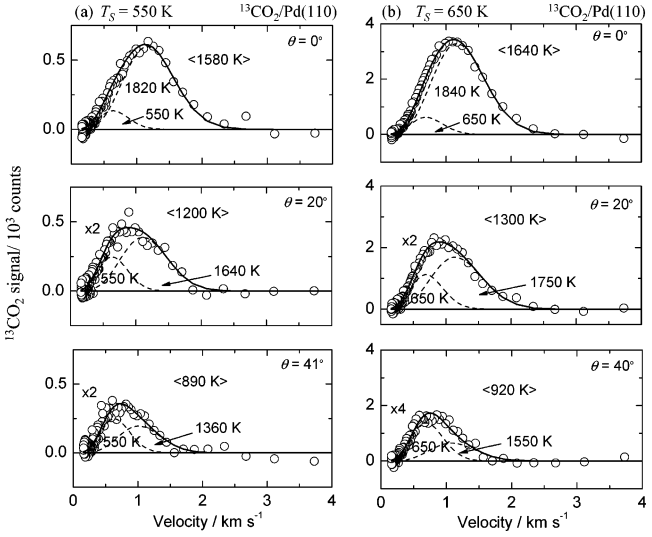

Figure 7. Velocity distributions of desorbing $^{13}CO_2$ at various desorption angles in a steady-state $^{14}NO + {}^{13}CO$ reaction on Pd(110) at the total pressure of 7.5×10^{-5} Torr (^{14}NO:^{13}CO = 1:1) and at (a) $T_S = 550$ K and (b) $T_S = 650$ K. The angle θ was scanned in the plane along the [001] direction. The average kinetic energy is given in $\langle\ \rangle$ in temperature units. Typical deconvolutions into a fast component and a slow component are given by broken curves. The translational temperature of the fast component is also given.

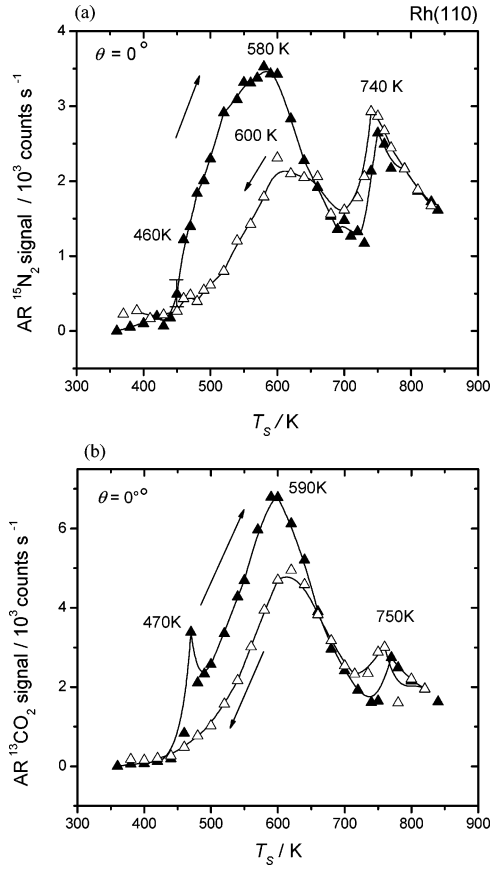

Figure 8. Steady-state AR signals at the surface normal of (a) $^{15}N_2$ and (b) $^{13}CO_2$ as a function of T_S at the total pressure of 7.5×10^{-5} Torr (^{15}NO:^{12}CO = 1:1 or ^{14}NO:^{13}CO = 1:1) on Rh(110). The signals observed in the direction of the increasing surface temperature are designated by closed symbols, and those in the downward direction, by open symbols. The lines in the figure are "guides to the eye".

the fast components. The translational temperature of this remaining component reached about 3300−3500 K at $\theta = 40-50°$ (Figure 13).

The velocity distribution after the subtraction of the thermalized component was still broad, yielding the speed ratio (SR), defined as $(\langle v^2\rangle/\langle v\rangle^2 - 1)^{1/2}/(32/9\pi - 1)^{1/2}$, of 1.09 at 550 K and 1.34 at 650 K, even at the collimation position. Here, v is the velocity of the molecule, $\langle v\rangle$ is the mean velocity, and $\langle v^2\rangle$ is the mean square velocity. This SR value indicates the width of the distribution curve and yields unity when the distribution is in a Maxwellian form.[24] The SR yields in most cases values smaller than unity for the desorption component with a hyperthermal energy at the collimation angle; i.e., lower-velocity molecules are less populated than those at the Maxwellian distribution at the translational temperature. However, the velocity distribution of the fast components yields the SR value larger than unity, although the translational temperature is very high. This strongly suggests that the velocity distribution after the subtraction of the thermalized component still involves two or more desorption components.

(A.2) Deconvolution of Velocity Distribution. Generally, it is difficult to uniquely deconvolute one velocity distribution curve into two or more distribution curves because two parameters are required to construct each distribution curve on the basis of the modified Maxwellian form.[24] This distribution is in the form of

$$f(v) = v^3 \exp\{-(v - v_0)^2/\alpha^2\}$$

where $f(v)$ is the modified Maxwellian distribution function, v_o is the stream velocity, and α is the width parameter. The stream velocity determines the peak position of the distribution. This distribution function is widely used to describe observed velocity distributions. Of course, one parameter is enough to describe a Maxwellian form (when $v_o = 0$), but no suitable deconvolution is successful when only two Maxwellian forms with different temperatures are used. One of the best ways is to deconvolute into two modified Maxwellians form; in this case, only three parameters are separately determined by fitting the data points at high- and low-velocity sides. There are several ways to omit the remaining parameter. Here, we simply assume a common width parameter. In this case, the energy of the faster component would be somewhat underestimated, and that of the other should be somewhat overestimated because the faster component is likely to yield a smaller α value. The resultant deconvolutions are shown by broken curves in Figure 6. The fastest component obtained in this way yielded a translational temperature of 6250 K (1.02 eV) maximizing at $\theta = 40-50°$ (Figure 13) and the SR of 0.66. The second component showed around 2500 K (0.43 eV) and the SR = 0.9. There are significant differences in the velocity curves of desorbing N_2 between the present work and the previous one.[12] In the latter, no signals were noticed above 2.5 km s^{-1}. On the other hand, in the present work, the signal was still significant in the range of 2.5−4 km s^{-1}, yielding a new faster component. The observation of these high-velocity signals might be obscured in the high background in the previous work because of the small signal intensity at low reactant pressures.

The translational temperature of fast CO_2 was simply estimated by subtracting the thermalized component. The energy of the resultant fast component was maximized to 1840 K at the normal direction and decreased quickly with increasing desorption angle (Figure 13). This is only one-third of that of the fastest component of N_2.

(A.3) Rh(110). The velocity distributions of N_2 and CO_2 products on Rh(110) were close to each other. Both translational temperatures were maximized at the normal direction. The fast component of CO_2 after the subtraction of the thermalized

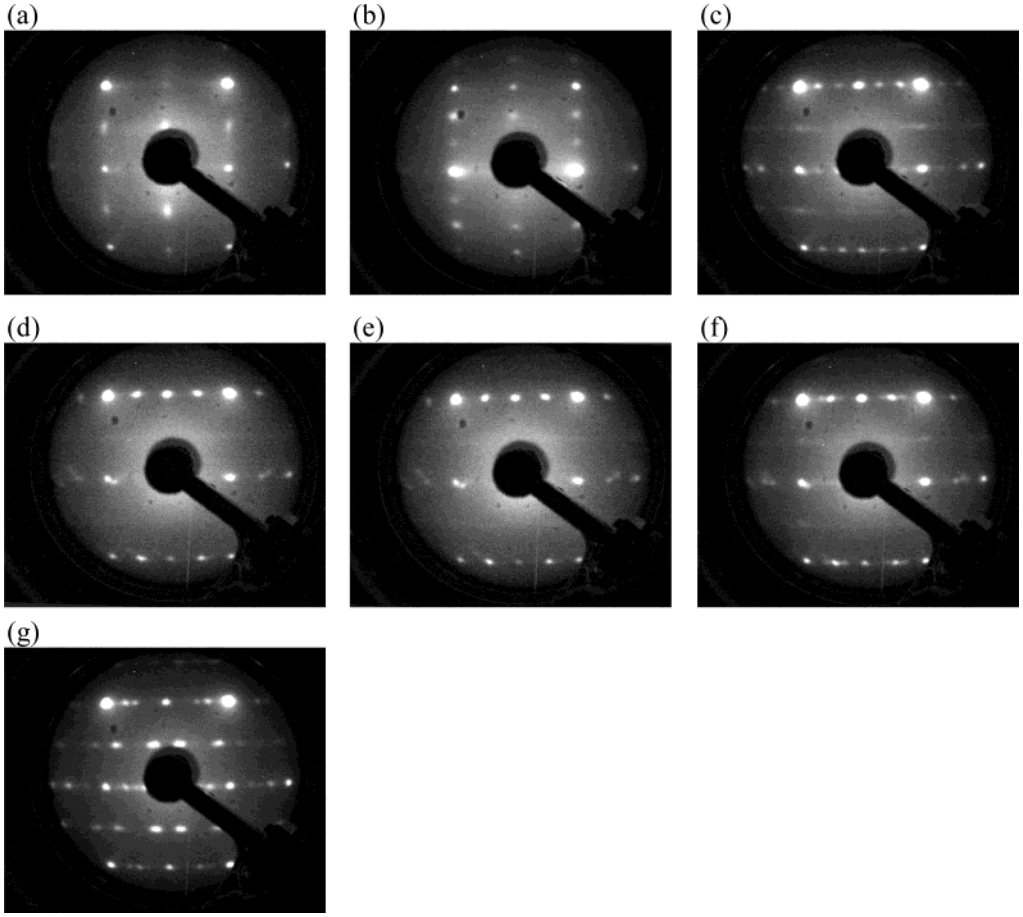

Figure 9. LEED patterns from Rh(110) in a steady-state NO + CO reaction. Diffraction patterns were recorded at the accelerating voltage of 85 eV at the total pressure of 1×10^{-7} Torr (NO:CO =1:1). T_S/K = (a) 360; (2×1)-N, (b) 380; (3×1)-N, (c) 580; (2×1)-N/(1×3)-O, (d) 740; (1×2)-O, (e) 840; (1×2)-O. In the decreasing temperature, (f) 600, c(4×2)+(1×2); and (g) 400, c(4×2)+(1×3).

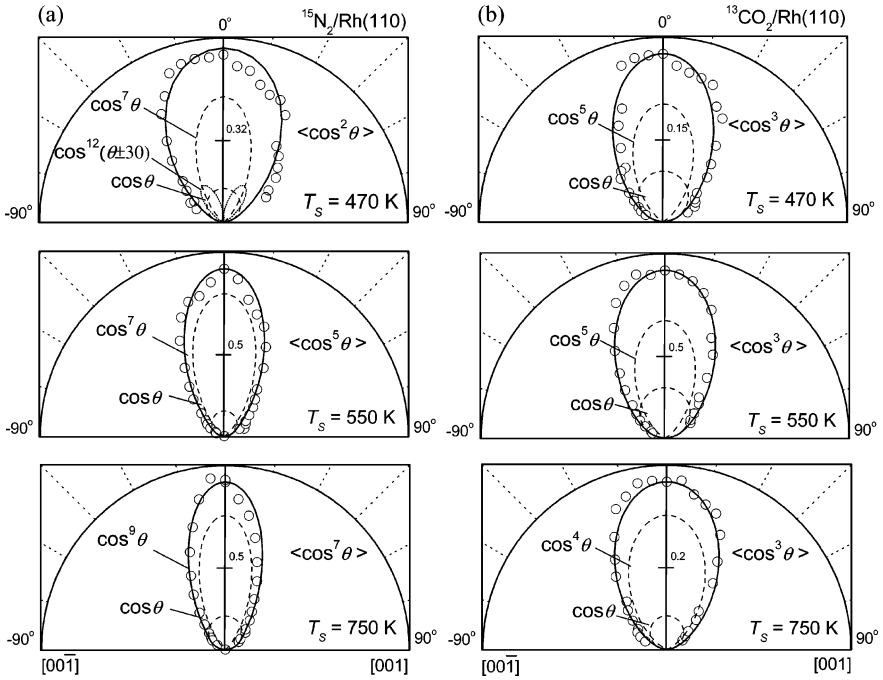

Figure 10. Angular distributions (shown in polar coordinates) on Rh(110) of desorbing (a) $^{15}N_2$ and (b) $^{13}CO_2$ in the plane along the [001] direction at different T_S values. The signal on the ordinate was normalized to that in the normal direction at 550 K. The reaction of NO + CO was at the steady state with the total pressure of 7.5×10^{-5} Torr (^{15}NO:^{12}CO = 1:1 or ^{14}NO:^{13}CO = 1:1). The apparent distribution is indicated in $\langle\ \rangle$. Typical deconvolutions are drawn by broken curves. The solid lines show the summation of components.

component reached 1940 K at the normal direction and decreased quickly with increasing desorption angle as shown by the broken curve in Figure 11b. This is consistent with the normally directed desorption.

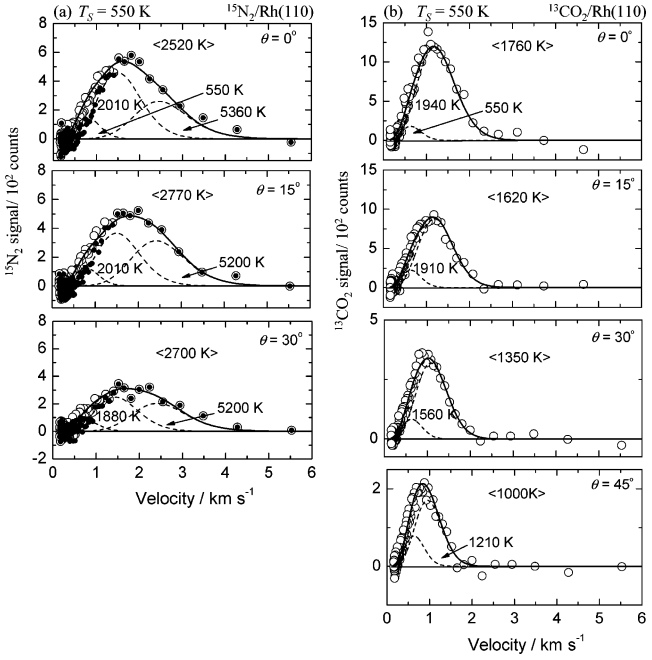

Figure 11. Velocity distributions at various desorption angles on Rh(110) of (a) $^{15}N_2$ and (b) $^{13}CO_2$ in a steady-state NO + CO reaction at the total pressure of 7.5×10^{-5} Torr (^{15}NO:^{12}CO = 1:1 or ^{14}NO:^{13}CO = 1:1) and at T_S = 550 K. The angle θ was scanned in the plane along the [001] direction. The average kinetic energy is given in $\langle\ \rangle$ in temperature units. Typical deconvolutions are given by broken curves. The translational temperature for each component is also given.

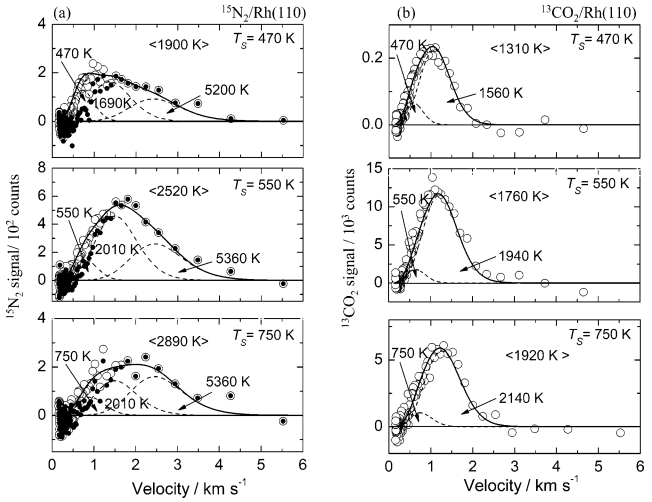

Figure 12. Velocity distributions at various temperatures on Rh(110) of (a) $^{15}N_2$ and (b) $^{13}CO_2$ in a steady-state ^{15}NO + ^{13}CO reaction at the total pressure of 7.5×10^{-5} Torr (^{15}NO:^{12}CO = 1:1 or ^{14}NO:^{13}CO = 1:1). The angle was fixed at θ = 0°. The average kinetic energy is given in $\langle\ \rangle$ in temperature units. Typical deconvolutions are given by broken curves. The translational temperature for each component is also given.

On the other hand, the fast component of desorbing N_2 after subtraction of the thermalized component reached 2520 K at the normal direction (Figure 11a). Surprisingly, this value did not decrease with increasing desorption angle. It increased from 2520 K at the normal direction to 2700 K at θ = 30°, although the flux decreased in this way. This suggests the presence of inclined desorption showing high velocity off the normal direction. In fact, the angular distribution became sharper at 750 K, suggesting the disappearance of the inclined component.

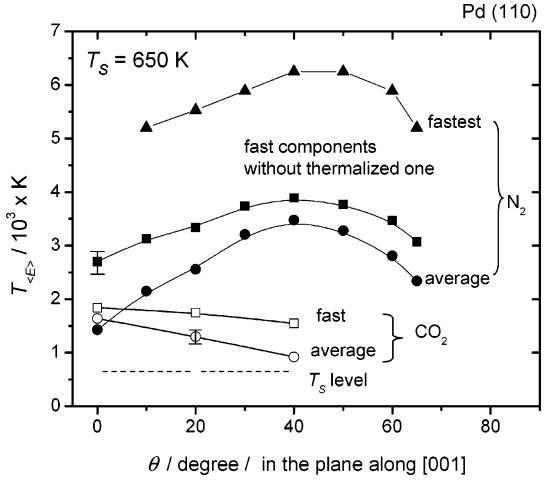

Figure 13. Translational temperature of $^{15}N_2$ (full marks) and $^{13}CO_2$ (opened marks) on Pd(110) versus the desorption angle in the plane along the [001] direction. The reaction was in the steady state at the total pressure of 7.5×10^{-5} Torr (^{15}NO:^{12}CO = 1:1 or ^{14}NO:^{13}CO = 1:1). The average value was calculated over all molecules before deconvolution of the velocity curve. The value for the fast component was estimated after deconvolution. The vertical bars indicate typical experimental errors. The lines in the figure are "guides to the eye".

(B) Reaction Pathways. The following steps were proposed to proceed NO decomposition on Pd and Rh surfaces.[8]

$$\mathrm{NO(g)} \rightarrow \mathrm{NO(a)} \quad \text{(i)}$$

$$\mathrm{NO(a)} \rightarrow \mathrm{N(a)} + \mathrm{O(a)} \quad \text{(ii)}$$

$$2\mathrm{N(a)} \rightarrow \mathrm{N_2(g)} \quad \text{(iii)}$$

$$\mathrm{N(a)} + \mathrm{NO(a)} \rightarrow \mathrm{N_2O(a)} \quad \text{(iv)}$$

$$\mathrm{N_2O(a)} \rightarrow \mathrm{N_2O(g)} \quad \text{(v)}$$

$$\mathrm{N_2O(a)} \rightarrow \mathrm{N_2(g)} + \mathrm{O(a)} \quad \text{(vi)}$$

To remove the surface oxygen, some reducing reagent, CO in the present case, is necessary for the catalytic cycle to proceed.

$$\mathrm{CO(g)} \rightarrow \mathrm{CO(a)} \quad \text{(vii)}$$

$$\mathrm{CO(a)} + \mathrm{O(a)} \rightarrow \mathrm{CO_2(g)} \quad \text{(viii)}$$

The oxygen removal step (viii) has been well-analyzed under steady-state conditions and also transient conditions. At temperatures above 400 K for steady-state reactions, O(a) on Pd(110) is quickly removed by CO. Desorbing CO_2 in CO oxidation on Pd(110) collimated sharply along the surface normal when O(a) $\gg$ CO(a), but it showed a cosine distribution when O(a) $\ll$ CO(a).[28,29] Similar phenomena were observed on Rh(110) except for bidirectional CO_2 desorption at the limited conditions.[32] Desorbing CO_2 in the NO + CO reaction showed angular and velocity distributions very similar to those in CO oxidation in the active region on both surfaces.

Steps (i), (ii), and (iii) have been well-characterized on Pd(110) and Rh(110). Step (ii) is in most cases rate-determining and subject to surface oxygen.[8] It proceeds above 420 K on Rh(110)[33] and 450 K on Pd(110) at the steady-state reaction. Desorbing N_2 from step (iii) sharply collimated along the surface normal.[7] Both Pd(110) and Rh(110) surfaces are converted into a missing-row form stabilized by oxygen when the surface is exposed to oxygen above 500 K.[31,34]

(C) Intermediate N_2O. The knowledge of steps (iv), (v), and (vi) in relation to $N_2O(a)$ is limited on noble metals. Step (iv), $N(a) + NO(a) \rightarrow N_2O(a)$, took place around 100 K on Pt(335), around 300−350 K on Rh(111), and above 400 K on Pd(110), where N(a) was formed from electron bombardments to NO(a) or by exciting $N_2(g)$.[7,21,35] N_2O decomposition, step (v), is sensitive to the kind of metal and its surface structure. On Pd((110),[13] Rh(110),[2,3] Ru(001), W(110),[36] Cu(110),[37] and stepped Ni(557),[38] the dissociation proceeds at or below 100 K. Incident N_2O was decomposed on Ni(110), Ni(100), and Rh(110) below 200 K[39,40] but not on Rh(111).[41] $N_2O(a)$ was desorbed at 90−120 K on Pt(111),[42] Ir(111),[43] Ni(111),[44] and Ag(111)[45] without dissociation. On Pt(335) = [(S)4(111)×(001)], step (iii), $2N(a) \rightarrow N_2(g)$, takes place around 400 K, showing high reactivity of surface nitrogen on platinum.[35] On Rh(110), Rh(100), and Rh(111), N_2O formation was observed in a steady-state NO + CO reaction at NO pressures above 10^{-2} Torr.[46]

$N_2O(a)$ was proposed to adsorb via its terminal N atom on metal surfaces in a standing form or in an inclined one.[42−45,47] Prior to decomposition, N_2O must lie to release oxygen on the surface. Ohno et al. proposed that N_2O is oriented along the [001] direction before decomposition and then the nascent N_2 receives repulsive forces along the ruptured N_2−O axis.[11] This aligned N_2O in the [001] direction was first proposed on Pd-(110)(1×1) as the precursor of inclined N_2 emission. The thermal decomposition of adsorbed N_2O is completed below 160 K on both Rh(110) and Pd(110); however, the presence of short-lived N_2O is not necessarily ruled out in the steady-state NO + CO reaction, even above 500 K, because adsorbed N_2O can be stabilized by surface oxygen.[3,48] A recent density functional theory (DFT) calculation with a generalized gradient approximation by Kokalj shows that the parallel form of N_2O on Pd(110) is in a bending configuration, bridging atomic troughs extending in the $[1\bar{1}0]$ direction.[49,50] It is as stable as a standing or tilting form with bonding via the terminal nitrogen atom. Recent near-edge X-ray absorption fine-structure spectroscopy (NEXAFS) measurements of N_2O on Pd(110) around 60 K showed remarkable anisotropy in the X-ray polarization dependence of two π resonance (N 1s $\rightarrow 3\pi^*$) NEXAFS peaks.[51] This suggests that the major N_2O is lying along the [001] direction and a minor species is standing, which is consistent with the DFT results.

The angular distribution of desorbing N_2 in the thermal decomposition of N_2O on Pd(110) was sharply collimated at 40−50° off the surface normal in the plane along the [001] direction.[13] The product N_2 showed high excess translational energy.[11,14] Both angular and velocity distributions are very similar to those observed in the steady-state NO + CO reaction on Pd(110) in the present work. We conclude that the inclined N_2 desorption comes from the intermediate N_2O decomposition in the steady-state NO + CO reaction.

(D) Inclined N_2 Desorption. Adsorbed N_2O is partly decomposed on Rh(110) even around 60 K, as confirmed by recent NEXAFS measurements.[52] The angular distribution of desorbing product N_2 in N_2O decomposition on this surface was more complex than that on Pd(110), as recently reported by AR-TPD.[2,3,6] When the clean surface was exposed to N_2O, the product N_2 desorption in the subsequent TPD procedure collimated along about 70° off the surface normal toward the [001] direction. This desorption was proposed to be due to the decomposition of surface-parallel N_2O oriented along the [001] direction. The N_2O decomposition was largely retarded on oxygen-covered Rh(110). The surface reactivity toward the N_2O decomposition was recovered after being heated above 1100 K. However, the collimation of desorbing N_2 on the resultant surface shifted only about 30° off the normal in the plane along the [001] direction. The desorption mechanism of this 30° component is not clear at present. The adsorption structure of declining N_2O, which interacts with the oxygen-modified site through the oxygen end, might be induced.

In fact, such inclined N_2O was predicted on positively charged Ag clusters.[53] This kind of positive metal atoms may be induced in rhodium oxides.[54] Such an adsorption structure of N_2O has never been proposed on clean noble metals.

Here, we may expect the contribution of this inclined desorption of N_2 in the steady-state NO + CO reaction because of the presence of surface oxygen.

However, we could not find N_2O formation on Rh(110) in the pressure range of 10^{-7}−10^{-4} Torr of NO and T_S = 300−800 K. The possibility of N_2O formation on Rh(110) cannot be completely ruled out because of the rapid decomposition on this surface and the observed sharpening of the angular distribution of desorbing N_2 at higher temperatures, which suggests the presence of inclined desorption. Furthermore, this possibility is also supported by the slow decay of the fast component with increasing desorption angle, as seen in Figure 11a. Thus, the angular distribution at T_S = 470 K was deconvoluted into three components, a $\cos^7(\theta)$ form, a $\cos(\theta)$ form, and the inclined $\cos^{12}(\theta \pm 30)$ form, as shown by the broken curves. Here, the deconvolution was performed by assuming the maximum contribution of the inclined component on Rh(110).

N(a) on Rh(110) is not highly reactive with NO(a); rather, it is reactive with N(a), forming $N_2(g)$. This suggests that the reactivity of N(a) is enhanced at high pressures because of the significant N_2O formation at high pressures. This enhancement is not necessarily induced by increased NO(a) or N(a) population. It may be enhanced by subsurface oxygen (or in oxide forms) or nitrogen.

(E) Branching of Surface-Nitrogen Removal. On Pd(110), the three removal pathways of surface nitrogen are operative: (I) through the associative process of N(a), i.e., $2NO(a) \rightarrow 2N(a) + 2O(a) \rightarrow N_2(g) + 2O(a)$; (II) via the intermediate decomposition of $N_2O(a)$, i.e., $2NO(a) \rightarrow O(a) + N(a) + NO(a) \rightarrow N_2O(a) + O(a) \rightarrow N_2(g) + 2O(a)$; and (III) through the desorption of $N_2O(a)$, i.e., $2NO(a) \rightarrow O(a) + N(a) + NO(a) \rightarrow N_2O(a) + O(a) \rightarrow N_2O(g) + O(a)$. Here, the removal of O(a) as CO_2 is omitted for simplicity. According to these reaction pathways, the product ratio must be $CO_2{:}N_2{:}N_2O = (2x + 2y + z){:}(x + y){:}z$, where x and y represent the progress of N_2 formation in the former two processes, I and II, and z indicates that of N_2O formation in the latter, III. The above-observed value on Pd(110) at 600 K is 5:2:1, consistent with this stoichiometry, yielding the ratio of 2:1 for $(x + y){:}z$. This ratio and the quantity of $[CO_2]/\{2[N_2] + [N_2O]\}$ are shown in Figure 14a as a function of the surface temperature. $[CO_2]$, $[N_2]$, and $[N_2O]$ designate the amount of produced CO_2, N_2, and N_2O, respectively, estimated from either AI or AR signals. The latter quantity should always be unity when no other reactions take place. This was confirmed for the observed values from the AI signals, as shown by open squares in Figure 14a. The values are scattered around unity because of the large error involved in the AI−N_2 signal. The $(x + y){:}z$ ratio represents the branching of $N_2{:}N_2O$ formation. The observed ratio steeply increased with increasing temperature above around 600 K; at higher surface temperatures, the N_2O formation was relatively more suppressed than the total N_2 formation. However, this branching parameter does not present how much N_2 is formed through the N_2O intermediate

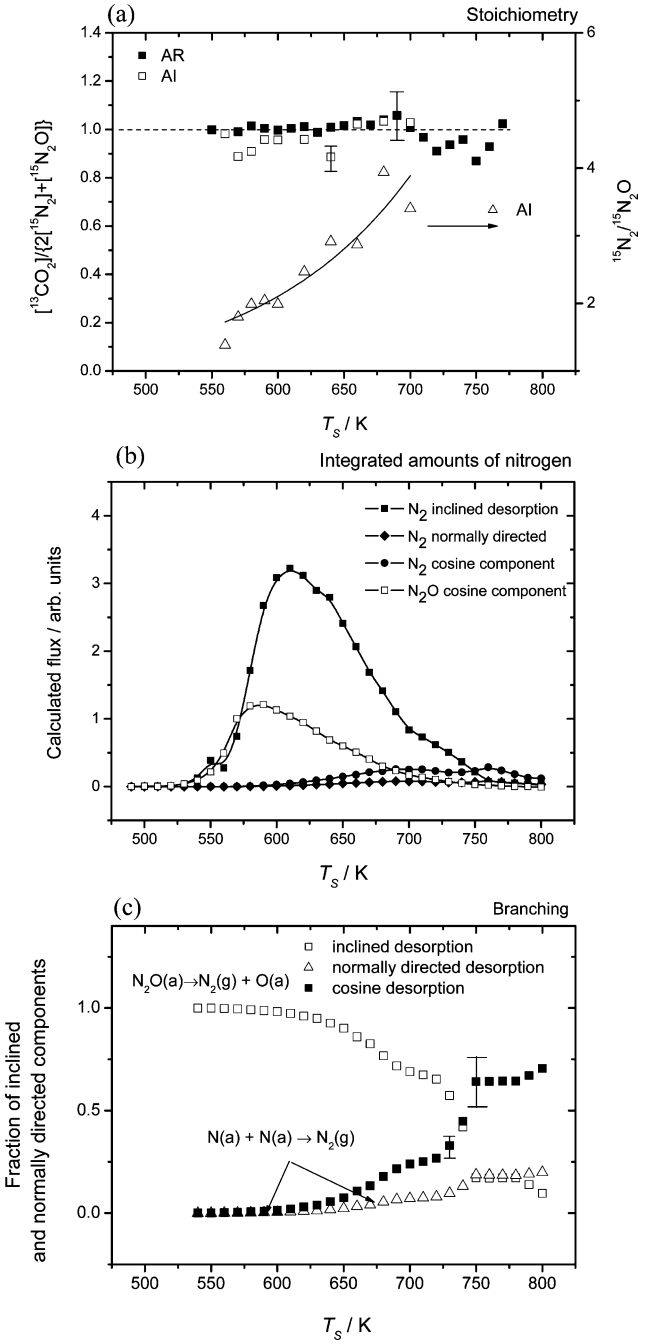

Figure 14. Stoichiometry and branching of the steady-state NO + CO reaction on Pd(110) at the total pressure of 7.5×10^{-5} Torr with a ^{15}NO:^{12}CO = 1:1 or ^{14}NO:^{13}CO = 1:1 mixture. (a) Ratio of the amount of $^{13}CO_2$ to that of ($2^{15}N_2 + {}^{15}N_2O$) calculated from (□) AI signals and (■) AR signals. The amount of $^{15}N_2$ from the AR signals was estimated by assuming the value of 14 for the power of the power series of the desorption angle in the inclined plane passing the collimation position and along the [1$\bar{1}$0] direction (see text). The branching ratio by ($^{15}N_2$):($^{15}N_2O$) is also shown. (b) Integrated amounts of nitrogen evolved in different ways: (■) $^{15}N_2$ inclined desorption; (◆) normally directed desorption; (●) cosine component; and (□) $^{15}N_2O$ in a cosine distribution. (c) Branching of $^{15}N_2$ formation. Fractions of $^{15}N_2$ formation: (□) through the intermediate $^{15}N_2O$ (inclined desorption); (△) through the associative process of N(a) (the normally directed desorption); and (■) the thermalized cosine desorption. The former process prevails at low temperatures, whereas, at high temperatures, the cosine component becomes predominant. Vertical bars indicate experimental errors. The lines in the figure are "guides to the eye".

pathway; i.e., the values of *x* and *y* are not separately determined. In the following analysis, we separately discuss these quantities, including the thermalized component, and show the degree to which the above two pathways, I and II, share the total N_2 yield. The branching in these two pathways can be estimated from angular distribution analysis. The observed angular distribution in the plane along the [001] direction was approximated as $0.95\{\cos^{28}(\theta + 41) + \cos^{28}(\theta - 41)\} + 0.03\cos^5(\theta) + 0.07\cos(\theta)$ at $T_S = 550$ K. The prefactors indicate the relative intensity. The contribution of the cosine component was estimated from the deconvolution of the velocity distributions. Below 600 K, N_2 is mostly desorbed through the inclined way. At 650 K, the distribution became $0.85\{\cos^{28}(\theta + 40) + \cos^{28}(\theta - 40)\} + 0.16\cos^5(\theta) + 0.16\cos(\theta)$; i.e., the normally directed components were enhanced. This tendency became clearer at higher temperatures, indicating a sharing shift in the reaction pathways. At higher temperatures, the surface nitrogen removal was highly contributed from the associative process of N(a).

TABLE 1: Anisotropic Desorption Parameters on Pd(110)

direction	CO_2	N_2 (inclined)	N_2 (normally)	N_2 (cosine)
[001]	$\cos^{15}(\theta)$	$\cos^{28}(\theta)$	$\cos^5(\theta)$	$\cos^1(\theta)$
[1$\bar{1}$0]	$\cos^3(\theta)$	$\cos^{14}(\theta)^a$	$\cos^5(\theta)$	$\cos^1(\theta)$
refs	this work,[55]	this work,[7]	this work	this work

[a] This sharpness represents the angle dependence in the declining plane passing the collimation position and along the [1$\bar{1}$0] direction.

The total amount of CO_2 produced was estimated from the AR-signal intensity at the collimation angle, the sharpness of the angular distribution around the collimation axis, and the mass sensitivity correction due to velocity. The total amount of desorbing species in the form of $\cos^n(\theta)\cos^m(\theta)$ is given by

$$Q = I_0(n+1)^{-1/2}(m+1)^{-1/2}$$

where *Q* is the total amount and *n* and *m* are the power value of the power series of $\cos(\theta)$ in the plane along the definite crystal azimuth and that perpendicular to it, respectively.[25] By considering the velocity differences among N_2 and N_2O and the anisotropy of the angular distribution around the collimation axis for N_2,[5,15,55] the formation of N_2 in the inclined way, the normally directed form, and the cosine form can be separately estimated. The amounts of CO_2 and N_2O were also estimated from the AR signals in a similar way. The used desorption parameters of CO_2 and N_2 are summarized in Table 1.

The results at the 7.5×10^{-5} Torr of the (1:1) mixture are shown in Figure 14b. The N_2 formation in each pathway was separately estimated. The results were again examined by the stoichiometry in Figure 14a. The contribution from the normally directed component in a $\cos^5(\theta)$ form is always minor because of the formation in a small amount. The anisotropic distribution of desorbing CO_2 has been well-studied and is shown in Table 1.[9] The distribution of desorbing N_2 was frequently assumed to be symmetric around the collimation axis at about 40° because of the difficulty in getting reliable data of angle-resolved measurements in the inclined plane passing the collimation position. To get the stoichiometry, the power in the power series of the cosine of the desorption angle along the [1$\bar{1}$0] direction was adjusted to the value of 14 ± 5 at 600 K. It agreed well with the report by Ikai and Tanaka.[20]

Below 600 K, N_2 is mostly formed from the N_2O decomposition, and N_2O formation is also significant. Above this temperature, both the N_2 formation from N_2O(a) and the N_2O desorption decrease rapidly, whereas the N_2 signal at the normal direction over that shared by the former process becomes noticeable. The N_2 desorption in the cosine form increases more

rapidly. The resultant branching of N_2 formation is shown in Figure 14c. The results above 750 K involved large uncertainty. In the figure, the inclined desorption represents the N_2 emission from the reaction pathway II through the decomposition of intermediate N_2O. The normally directed component in a $\cos^5(\theta)$ form is ascribed to the reaction pathway I via the N(a) associative process. The remaining cosine component becomes major at high temperatures. This cosine component showed similar kinetic behavior to that of pathway I with respect to the surface temperature and the P_{CO}/P_{NO} ratio, suggesting that it was also due to the associative process. There must be a mechanism whereby the associative process is likely to yield a thermalized component. In general, the N_2 formation through the associative process of N(a) is enhanced at higher temperatures.

On Rh(110), the N_2 formation mostly proceeds through the associative process in the NO pressure range studied, although the contribution from the inclined N_2 desorption pathways is highly possible at lower temperatures. AR-SSD measurements are desirable in the pressure range of $10^{-4}-10^{-2}$ Torr and at lower temperatures.

(F) Desorption Dynamics. Two or three fast-desorption components were already found in desorbing product N_2 molecules in the NO + CO reaction on Pt(100),[56] in the N_2O decomposition on Pd(110),[11,14] and in the NO decomposition on Pd(110).[11,12] These N_2 molecules have very high velocity; furthermore, their velocity distribution curve is commonly wider than that of the Maxwellian form at a definite temperature. These fast components were proposed to be due to the different vibrational states because of the energy difference close to the vibrational excitation of N_2, 0.28 eV (1610 K or 26.9 kJ); i.e., the faster component is in the lower vibrational energy state. The velocity distribution of N_2 in the present work is wide enough to involve several vibrational excited levels. In fact, desorbing N_2 in the associative process of N(a) on Cu(111), Ag(111), and Ru(001) showed very wide translational energy distributions and high populations of vibrational excited states.[57−59] Higher time-resolution TOF measurements in the state-selective form are required.[60]

The composition with respect to different velocity components of desorbing N_2 was, surprisingly, fairly insensitive toward the desorption angle on both Rh(110) and Pd(110). Here are several possibilities for this occurrence. On Rh(110), the presence of inclined desorption in the reaction $N_2O(a) \rightarrow N_2(g) + O(a)$ is highly possible.[3,6] The observed $T_{\langle E\rangle}$ would be insensitive to the desorption angle if the inclined component of N_2 contributed to $T_{\langle E\rangle}$ at large desorption angles because the translational energy should be maximized at the collimation angle. In fact, the angular distribution becomes sharp at higher temperatures (Figure 10). The suppression of the inclined component is reasonably expected at higher temperatures. On the other hand, the angular distribution representing a single process usually becomes broader at higher temperatures, as seen in the CO_2 velocity distributions on both Pd(110) and Rh(110), because of the enhanced thermal motion.[5,9]

For the inclined desorption on Pd(110), the following possibilities are expected: (1) significant anisotropy in velocity distributions of each desorption component is present,[5] i.e., a rapid decrease of the fastest component would be observed in the plane along the $[0\bar{1}1]$ direction rotated 90° from the present azimuth; (2) a new energy transfer mechanism is operative, i.e., the energy transfer from the transition state into the translational mode may be preferred at larger shifts from the collimation angle, whereas desorbing N_2 around the collimation angle receives more energy into the vibrational modes. This branching change may compensate the rapid decrease of the fast component at large desorption angles.

Such highly excited molecules originate from a large energy dissipation in the N_2 desorption processes. For the process of $N_2O(a) \rightarrow N_2(g) + O(a)$, the energy which the product N_2 can carry out is presented by ΔE_T, which is given as $\Delta E_T = E_{N2(g)} + E_{O(a)} - E_{N2O(a,TS)}$, where $E_{N2(g)}$, $E_{O(a)}$, and $E_{N2O(a;TS)}$ are the potential energies of $N_2(g)$, O(a), and the transition state of N_2O-(a) dissociation, respectively. By assuming 400−500 kJ mol^{-1} as the bond energy of O−metal,[61] the available energy was estimated to be 240−340 kJ mol^{-1} because the dissociation of $N_2O(g) \rightarrow N_2(g) + O(g)(^3P)$ is endothermic by about 160 kJ mol^{-1} and the heat of adsorption of N_2O on both Pd(110) and Rh(110) is close to the activation energy of $N_2O(a)$ dissociation.[5] In this process, the emitted energy mostly comes from the metal−O bond formation. In the associative processes of N(a), the released energy may become higher because of the high bond energy of N−N (945 k J mol^{-1}) and the low binding of N−noble metals.[58−60]

V. Summary

The angular and velocity distributions of desorbing products N_2 and CO_2 were successfully analyzed in the steady-state NO + CO reaction on Pd(110) and Rh(110) in a wide range of NO pressures by means of angle-resolved product desorption with cross-correlation time-of-flight techniques and LEED observations. The following results were obtained.

(1) On Pd(110), N_2 desorption was split into two inclined components collimating at ±40° in the plane along the [001] direction. On the basis of the close similarity of angular and velocity distributions in N_2O decomposition on Pd(110), the inclined N_2 formation is proposed to originate from the N_2O intermediate. At low temperatures, the pathway through the N_2O intermediate prevails, and, above 720 K, the associative nitrogen desorption starts to dominate.

(2) N_2 desorption on Rh(110) was sharply collimated along the surface normal in a wide temperature region, indicating that N(a) is mostly removed through the associative process.

(3) On both surfaces, the translational temperature of desorbing N_2 was very high, reaching about 2500−3500 K. On the other hand, the CO_2 desorption always collimated along the surface normal on both surfaces with the translational temperature in the range of 1600−2000 K.

Acknowledgment. I.I.R. is indebted to the Ministry of Education, Sports, and Culture of Japan for her scholarship (2001−2004). This work was partly supported by a 1996 COE special equipment program of the said Ministry. It was also supported in part by Grant-in-Aid No. 13640493 for General Scientific Research from the Japan Society for the Promotion of Science. The authors thank Ms. Atsuko Hiratsuka for drawing the figures.

References and Notes

(1) Rahkamaa, K.; Salmi, T. *Chem. Eng. Sci.* **1999**, *54*, 4343.

(2) Horino, H.; Rzeźnicka, I.; Kokalj, A.; Kobal, I.; Hiratsuka, A.; Ohno, Y.; Matsushima, T. *J. Vac. Sci. Technol., A* **2002**, *20*, 1592.

(3) Imamura, K.; Horino, H.; Rzeźnicka, I.; Kobal, I.; Kokalj, A.; Ohno, Y.; Nieuwenhuys, B. E.; Hiratsuka, A.; Matsushima, T. *Surf. Sci.*, **2004**, in press.

(4) Matsushima, T. *Catal. Surv. Jpn.* **2002**, *5*, 71.

(5) Matsushima, T. *Surf. Sci. Rep.* **2003**, *52*, 1.

(6) Liu, S.; Horino, H.; Kokalj, A.; Rzeźnicka, I.; Imamura, K.; Ma, Y.-S.; Kobal, I.; Ohno, Y.; Hiratsuka, A.; Matsushima, T. *J. Phys. Chem. B* **2004**, *108*, 3828.

(7) Ikai, M.; Tanaka, K. I. *J. Phys. Chem. B* **1999**, *103*, 8277.
(8) Garin, F. *Appl. Catal., A* **2001**, *222*, 183.
(9) Matsushima, T. *Heterog. Chem. Rev.* **1995**, *2*, 51.
(10) Kobal, I.; Rzeźnicka, I.; Matsushima, T. *Recent Research Developments in Physical Chemistry*; Transworld Research Network: Trivandrum, India, 2002; Vol. 6, p 391.
(11) Ohno, Y.; Kimura, K.; Bi, M.; Matsushima, T. *J. Chem. Phys.* **1999**, *110*, 8221.
(12) Kobal, I.; Kimura, K.; Ohno, Y.; Matsushima, T. *Surf. Sci.* **2000**, *445*, 472.
(13) Horino, H.; Liu, S.; Hiratsuka, A.; Ohno, Y.; Matsushima, T. *Chem. Phys. Lett.* **2001**, *341*, 419.
(14) Ohno, Y.; Kobal, I.; Horino, H.; Rzeźnicka, I.; Matsushima, T. *Appl. Surf. Sci.* **2001**, *169/170*, 273.
(15) Kobal, I.; Kimura, K.; Ohno, Y.; Horino, H.; Rzeznicka, I.; Matsushima, T. *Stud. Surf. Sci. Catal.* **2000**, *130*, 1337.
(16) Arumainayagam, C. R.; Madix, R. J. *Prog. Surf. Sci.* **1991**, *38*, 1.
(17) Colonell, J. I.; Gibson, K. D.; Sibener, S. J. *J. Chem. Phys.* **1996**, *104*, 6822.
(18) Ikai, M.; Tanaka, K.-I. *Surf. Sci.* **1996**, *357/358*, 781.
(19) Ikai, M.; Janssen, N. M. H.; Nieuwenhuys, B. E.; Tanaka, K. *J. Chem. Phys.* **1997**, *106*, 311.
(20) Ikai, M.; Tanaka, K.-I. *J. Chem. Phys.* **1999**, *110*, 7031.
(21) Belton, D. N.; DiMaggio, C. L.; Schmieg, S. J.; Simon Ng, K. Y. *J. Catal.* **1995**, *157*, 559.
(22) Zaera, F.; Gopinath, C. S. *Chem. Phys. Lett.* **2000**, *332*, 209.
(23) Rzeźnicka, I.; Moula, Md. G.; Morales, L.; Ohno, Y.; Matsushima, T. *J. Chem. Phys.* **2003**, *119*, 9829.
(24) Comsa, G.; David, R. *Surf. Sci. Rep.* **1985**, *5*, 145.
(25) Cao, G.; Moula, Md. G.; Ohno, Y.; Matsushima, T. *J. Phys. Chem. B* **1999**, *103*, 3235.
(26) Rzeźnicka, I.; Matsushima, T. *Chem. Phys. Lett.* **2003**, *377*, 279.
(27) Ehrlich, G. In *Chemistry and Physics of Solid Surfaces*; Vancelow, R., How, R., Eds.; Springer-Verlag: Berlin, Heidelberg, Germany, 1988; Vol. VII, p 1.
(28) Moula, Md. G.; Wako, S.; Cao, G.; Kimura, K.; Ohno, Y.; Kobal, I.; Matsushima, T. *Phys. Chem. Chem. Phys.* **1999**, *1*, 3677.
(29) Wako, S.; Moula, Md. G.; Cao, G.; Ohno, Y.; Kobal, I.; Matsushima, T. *Langmuir* **2000**, *16*, 2689.
(30) Lizzit, S.; Comelli, G.; Hofmann, Ph.; Paolucci, G.; Kiskinova, M.; Rosei, R. *Surf. Sci.* **1992**, *276*, 144.
(31) Dhanak, V. R.; Comelli, G.; Cautero, G.; Paulucci, G.; Prince, K. C.; Kiskinova, M.; Rosei, R. *Chem. Phys. Lett.* **1992**, *188*, 237.
(32) Rzeźnicka, I.; Matsushima, T. *J. Phys. Chem. B* **2003**, *107*, 8479.
(33) Bowker, M.; Guo, Q.; Li, Y.; Joyner, R. W. *J. Chem. Soc., Faraday Trans.* **1995**, *91*, 3663.
(34) Dhanak, V. R.; Comelli, G.; Paolucci, G.; Prince, K. C.; Rosei, R. *Surf. Sci.* **1992**, *260*, L24.
(35) Wang, H.; Tobin, R. G.; DiMaggio, C. L.; Fisher, G. B.; Lambert, D. K. *J. Chem. Phys.* **1997**, *107*, 9569.
(36) Umbach, E.; Menzel, D. *Chem. Phys. Lett.* **1981**, *84*, 491.
(37) Ceballos, G.; Wende, H.; Baberschke, K.; Arvanitis, D. *Surf. Sci.* **2001**, *482*−*485*, 15.
(38) Kodama, C.; Orita, H.; Nozoye, H. *Appl. Surf. Sci.* **1997**, *121/122*, 579.
(39) Sau, R.; Hudson, J. B. *J. Vac. Sci. Technol.* **1981**, *18*, 607.
(40) Hoffman, D. A.; Hudson, J. B. *Surf. Sci.* **1987**, *180*, 77.
(41) Li, Y.; Bowker, M. *Surf. Sci.* **1996**, *348*, 67.
(42) Avery, N. R. *Surf. Sci.* **1983**, *131*, 501.
(43) Cornish, J. C. L.; Avery, N. R. *Surf. Sci.* **1990**, *235*, 209.
(44) Väterlein, P.; Krause, T.; Bässler, M.; Fink, R.; Umbach, E.; Taborski, J.; Wüstenhagen, V.; Wurth, W. *Phys. Rev. Lett.* **1996**, *76*, 4749.
(45) Schwaner, L.; Mahmood, W.; White, J. M. *Surf. Sci.* **1996**, *351*, 228.
(46) Herman, J. S.; Peden, C. H. F.; Schmieg, S. J.; Belton, D. N. *Catal. Lett.* **1999**, *62*, 131.
(47) Haq, S.; Hodgson, A. *Surf. Sci.* **2000**, *463*, 1.
(48) Huang, H. H.; Seet, C. S.; Zou, Z.; Xu, G. Q. *Surf. Sci.* **1996**, *356*, 181.
(49) Kokalj, A.; Kobal, I.; Horino, H.; Ohno, Y.; Matsushima, T. *Surf. Sci.* **2002**, *506*, 196.
(50) Kokalj, A.; Kobal, I.; Matsushima, T. *J. Phys. Chem. B* **2003**, *107*, 2741.
(51) Horino, H.; Rzeźnicka, I.; Matsushima, T.; Takahashi, K.; Nakamura, E. *UVSOR Activity Report 2002*; Okazaki, Japan, 2003; p 209.
(52) Horino, H.; Rzeźnicka, I.; Matsushima, T.; Takahashi, K.; Nakamura, E. *UVSOR Activity Report 2002*: Okazaki, Japan, 2003; p 211.
(53) Zhanpeisov, N. U.; Martra, G.; Ju, W. S.; Matsuoka, M.; Coluccia, S.; Anpo, M. *J. Mol. Catal. A: Chem.* **2003**, *201*, 237.
(54) Yakovlev, A. L.; Zhidomirov, G. M.; Van Santen, R. A. *Catal. Lett.* **2001**, *75*, 45.
(55) Rzeźnicka, I.; Ohno, Y.; Horino, H.; Kobal, I.; Kimura, K.; Matsushima, T., *Proc. 9th Int. Heterog. Catal. Varna* **2000**, 97.
(56) Ohno, Y.; Sarawut, P.; Horino, H.; Kobal, I.; Hiratsuka, A.; Matsushima, T. *Chem. Phys. Lett.* **2003**, *373*, 161.
(57) Murphy, M. J.; Skelly, J. F.; Hodgson, A. *Chem. Phys. Lett.* **1997**, *279*, 112.
(58) Carter, R. N.; Murphy, M. J.; Hodgson, A. *Surf. Sci.* **1997**, *387*, 102.
(59) Murphy, M. J.; Skelly, J. F.; Hodgson, A.; Hammer, B. *J. Chem. Phys.* **1999**, *110*, 6954.
(60) Hodgson, H. *Prog. Surf. Sci.* **2000**, *63*, 1.
(61) Brown, W. A.; Kose, R.; King, D. A. *Chem. Rev.* **1998**, *98*, 797.